

Hierarchical Nanostructured ZnO with Nanorods Engendered to Nanopencils and Pin-Cushion Cactus with Its Field Emission Study

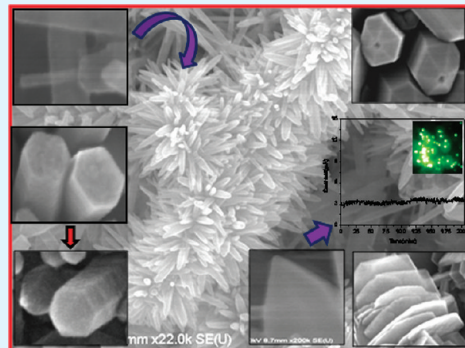
Sambhaji S. Warule,^{†,‡} Nilima S. Chaudhari,[†] Jalindar D. Ambekar,[†] Bharat B. Kale,^{*,†} and Mahendra A. More^{*,†}

[†]Centre for Materials for Electronics Technology (C-MET), Department of Information Technology, Govt. of India, Panchawati, off Pashan Road, Pune-411 008 India

[‡]Center for Advanced Studies in Materials Science and Condensed Matter Physics, Department of Physics, University of Pune, Pune-411 007, India

 Supporting Information

ABSTRACT: In the present investigation, we report the synthesis of highly crystalline ZnO nanorods engendered to pin-cushion cactus and 1D nanopencil like nanoforms on zinc (Zn) foil via a simple sonochemical assisted hydrothermal route. The work reported herewith is attractive for two reasons: (i) the facile one step solution approach assisted by prior ultrasonication converts nanorods/nanobelts into nanopencils, and (ii) the sharp and quasi-aligned ZnO nanopencils are potential field electron emitters. In addition, the controlled growth of pinhole like ZnO nanopencils and aligned hexagonal ZnO nanodisc was obtained. The changes in the growth rate, diameter, density, and surface area of highly oriented ZnO nanorods are examined. Considering the significances of such novel morphologies, technically detailed formation mechanism has been proposed. The field emission study of pin-cushion cactus like ZnO nanopencils was performed. Field emission measurements demonstrate remarkably low turn-on field which is explained on the basis of a sequential enhancement mechanism involving the consecutive stem and tip contribution. The Folwer–Nordheim (F–N) plot showed nonlinear behavior indicating the semiconducting nature of the emitter. Significantly, emission current is stable at the preset value of $3 \mu\text{A}$ over the period of 3 h. The simplicity of the synthesis route coupled with the promising emission properties is envisaged to be an important candidate for potential nanoelectronic devices. These unique imperative ZnO nanostructures may have potential for sensors, solar cell, photocatalysis, varistors, etc.



KEYWORDS: hierarchical nanostructures, ultrasonication, pin-cushion cactus, field emission

1. INTRODUCTION

Nanomaterials with unique nanostructures and morphologies are a current research area of interest due to their immense possibilities for a technological revolution.¹ The creation of nanomaterials via solution chemistry is a state of the art arrested crystal growth, leading to materials with respect to confinement in sizes and shape as well.^{2,3} Zinc oxide, having a wide band gap semiconductor (3.37 eV) with large exciton binding energy (60 meV), is one of the most promising functional materials. The 1D nanopencils/nails with prismatic tip may be superior for electronic application other than 1D ZnO nanostructures. Therefore, an investigation of such ZnO nanostructures with highly oriented, aligned, and ordered arrays has immense significance for the development of novel devices like field emission displays, solar cells, and other nanodevices.^{4–6} So far, several kinds of fabrication techniques, including thermal evaporation, vapor–liquid–solid (VLS) growth,⁷ metal–organic chemical vapor deposition (MOCVD),⁸ high pressure pulsed laser deposition,⁹ and the aqueous mediated synthesis,¹⁰ are used for synthesizing 1D ZnO nanomaterials. The aqueous mediated synthesis has the advantages of low temperature and simple equipment and being

achievable for large-area fabrication of different nanostructures. The growth of aligned ZnO nanorods and nanopencils on ZnO/Si in aqueous solution was reported.¹¹ The controlled growth of ZnO nanopagoda arrays with varied lamination and apex angles using ascorbic acid,¹² ZnO nanorods, and prism arrays in a large area on Zn substrate was reported at 160 °C.¹³ The engineering of nanotips in ZnO submicrorods and patterned arrays in ethylenediamine was also fabricated at 180 °C.¹⁴ In particular, ZnO nanorods have been investigated as electron field emitters due to their high temperature stability, large scale application, high aspect ratio, and low work function.^{15–19} The recent field emission of the 1D ZnO nanomaterials indicates that electrons are more easily emitted from the nanostructures having sharp tips than nanostructures with uniform diameter. Therefore, it is necessary to control the morphologies of the nanorods for improving their field emission properties. Recently, a two-step etching process (chemical and plasma etching process) for

Received: May 28, 2011

Accepted: August 4, 2011

Published: August 04, 2011

Table 1. Experimental Conditions for Synthesis of ZnO Samples

sample	ethanol/H ₂ O (mL)	ultrasonication period (min)	hydrothermal temperature (°C), reaction period (h)
I	80:20	45	
II	80:20	45	85 °C, 12 h
III	0:100	90	
IV	0:100	90	120 °C, 12 h

controlling the tip angle of the ZnO nanorods has been reported.²⁰ However, the two-step textured method is still complicated because it needs processing of film of the ZnO nanocrystals. Therefore, from the technology point of view, it is imperative to develop an alternative method to tackle the two step growth. Thus, we have recently reported a single step process to the controlled synthesis of the ZnO nanostructures using a sonochemical assisted hydrothermal route.²¹ Thus, herein, we demonstrate such a simple and expedient process useful to grow ZnO nanopencils from ZnO nanorods at low temperatures. It is noteworthy that the synthesis of self-assembled nanopencil like nanostructures originating from ZnO nanorods using a simple one-step sonochemical assisted hydrothermal route with promising field emission is hitherto unattempted.

In this communication, we report the fabrication of ZnO nanopencils from nanorods simply by tailoring the ultrasonication period before hydrothermal treatment. The as-synthesized pin-cushion cactus like ZnO nanopencils with a prismatic tip showed good field emission performance. This approach provides a convenient and simple technique for the manufacture of the novel 1D ZnO nanostructures with single crystal orientation suitable for fabricating various devices.

2. EXPERIMENTAL SECTION

Synthesis. The synthesis of ZnO nanostructures on Zn foil were performed by sonochemical treatment followed by a hydrothermal route. In the typical synthesis of Sample I, equimolar concentration (0.02 M) of zinc nitrate hexahydrate and hexamethylenetetramine (HMT) dissolved in a 100 mL mixture of ethanol/H₂O (8:2) at room temperature. Ultrasonication (20 kHz) was performed at an intensity of 39.5 W/cm² for 45 min. During the ultrasonication, precleaned Zn foils ($1 \times 1 \text{ cm}^2$) were dipped into the reaction bath so as to obtain growth of the ZnO nanostructures on it. After the sonication, the Zn foil was removed from the reactor and washed with distilled water (DW), followed by drying at 70 °C. In the case of the synthesis of Sample II, an ultrasonically irradiated solution of Sample I was immediately transformed into a Teflon lined stainless steel autoclave (100 mL capacity). Subsequently, the growth was carried out by suspending the Zn foil with a ZnO seed layer (Sample I) in a sealed autoclave filled with a reaction solution. The hydrothermal synthesis was carried out at 85 °C for 12 h. After completion of the reaction, the Zn foil was removed from the autoclave, washed with distilled water to remove the unreacted salt if any, and dried at 70 °C.

The same procedure has been employed for the syntheses of Samples III and IV. The detailed experimental parameters are furnished in Table 1.

Characterization. The phase identification of the as-synthesized products was performed by X-ray diffractometer (XRD, D8 Advance, Bruker AXS). The surface morphologies of the ZnO nanostructures were investigated by a field emission scanning electron microscope

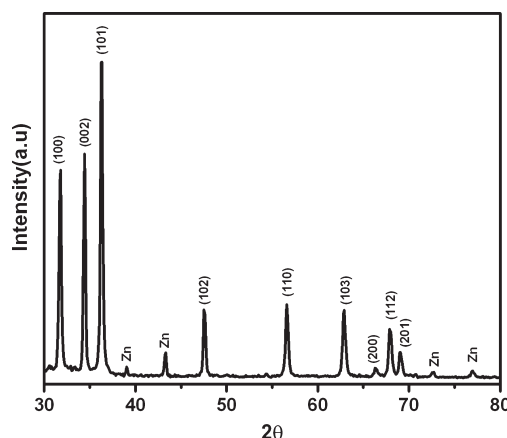


Figure 1. XRD spectra of Sample II.

(FESEM, Hitachi, S-4800). The morphology and crystalline nature of as-synthesized product was further studied by a high resolution transmission electron microscope (HRTEM, Tecnai G² 20 Twin, FEI). The optical properties were investigated from photoluminescence (PL) spectra recorded at room temperature using a Xenon lamp as the excitation source (photoluminescence Spectrometer; Perkin-Elmer-LS-55). The excitation wavelength of $\sim 325 \text{ nm}$ was used.

Field Emission Measurement. The field emission current versus applied voltage ($I-V$) and current versus time ($I-t$) characteristics were recorded in a planar diode configuration in a vacuum chamber evacuated to a base pressure of $\sim 1 \times 10^{-8} \text{ mbar}$. The ZnO film synthesized on Zn foil served as an emitter cathode. A semitransparent phosphor screen, used as an anode, was held parallel to the cathode at a distance of $\sim 1 \text{ mm}$. The details of the field emission system and vacuum processing of the chamber are reported elsewhere.²² The emission current data was acquired using auto ranging a Keithley 485 picoammeter, by varying the applied DC voltage between the cathode and the anode in steps of 40 V (0–40 kV, Spellman, USA). Care was taken to avoid any leakage current by ensuring proper grounding.

3. RESULTS AND DISCUSSION

The X-ray diffraction (XRD) pattern of a typical as-synthesized ZnO film (Sample II) is depicted in Figure 1. The XRD pattern exhibits a set of well-defined diffraction peaks which are in good agreement with the hexagonal wurtzite phase of ZnO (JCPDS 80-0075). Some characteristic diffraction peaks corresponding to Zn are attributed to Zn foil which is used as a substrate. The XRD spectra of other samples (i.e., I, III, IV, etc.) are given in the Supporting Information, S-I.

The morphologies of the as-synthesized films using a sonochemical route (Sample I) and followed by a hydrothermal route (Sample II) were examined with FESEM, and their typical images are shown in Figure 2. The surface morphology of the Sample I (Figure 2a) is a network of randomly oriented ZnO nanorods mostly parallel to the surface of substrate. The average diameter and length of these nanorods are observed to be 100 nm and 2 μm , respectively. These rods seem to be transparent which are clearly seen in the magnified image. (See Supporting Information, S-IIa.) After careful observation, the surface morphology of Sample II (Figure 2b) suggests that (a) the urchin-shaped ZnO nanostructures composed of ZnO nanorods are obtained at low temperature (85 °C) on the entire substrate surface, (b) the base of the nanorods is hexagonal, indicating crystal growth along the wurtzite *c* axis, and (c) the further growth leads to tapering of

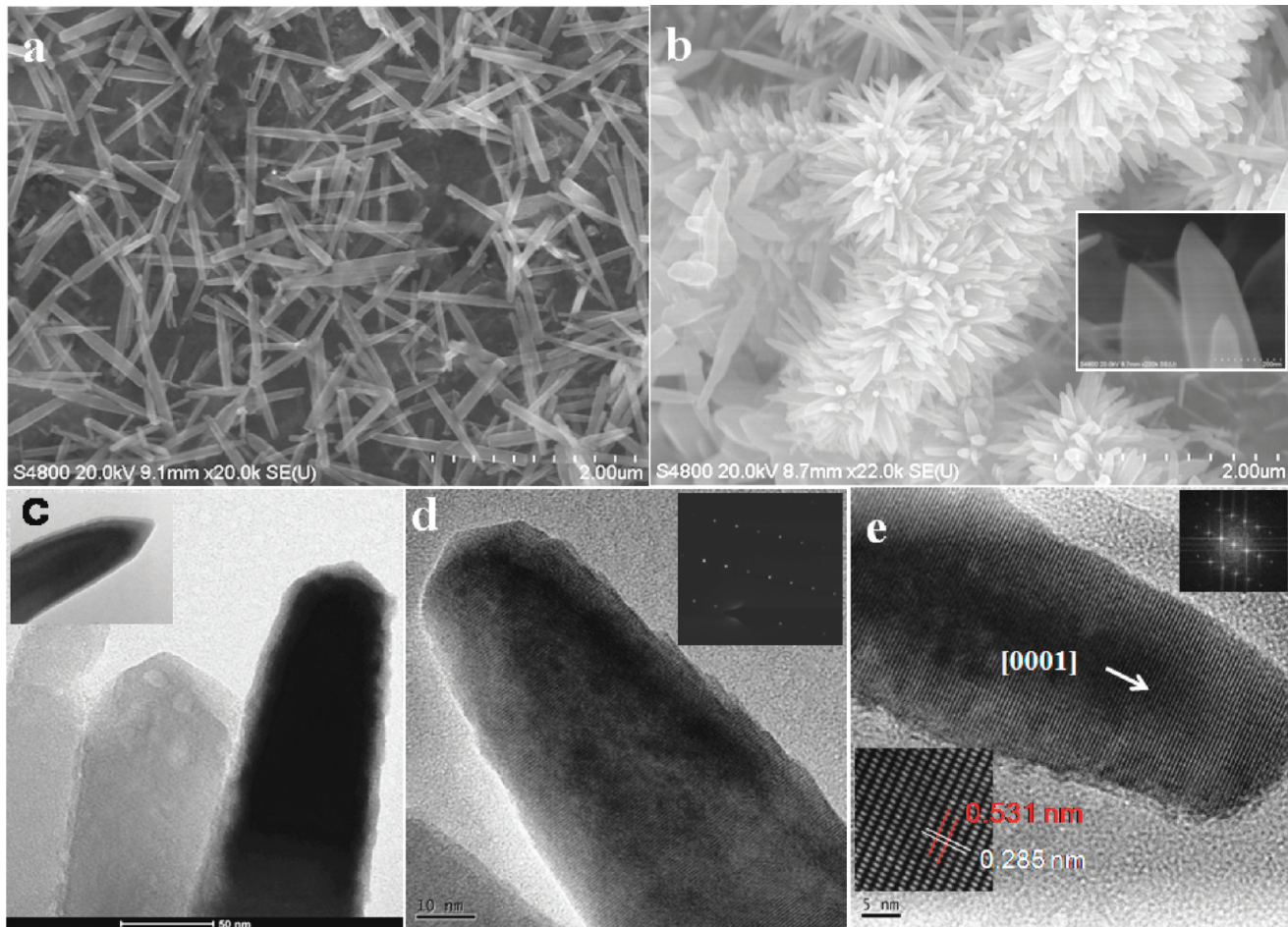


Figure 2. FESEM micrograph of Sample I (a) and Sample II (b). (c,d) TEM micrograph of Sample II with inset SAED and (e) HRTEM image of ZnO nanorod with inset FFTED pattern.

nanorods engendering into prismatic tip. Formation of similar chain-shaped ZnO nanostructures composed of hexagonal ZnO nanorods was achieved at 120 °C.²³ Hexagonal faceted ZnO nanopencils were grown perpendicular to a substrate. The pencils have an average diameter of 120 nm with length in micrometers. Careful observations of the micrograph (Figure 2a) reveal that seed layer plays the vital role in developing nanopencils. (Details are discussed in Growth Mechanism.) The morphology and the crystalline nature of the as-synthesized product were further investigated by TEM. Figure 2c shows the TEM image of the ZnO nanopencil (Sample II), having uniform stem with a sharp tip at one end (inset Figure 2c). The observed morphology of the nanopencils is also consistent with the FESEM observations. A typical selected area of the electron diffraction (SAED) pattern (inset of Figure 2d) exhibits sharp diffraction spots with the single crystal behavior of ZnO. A high resolution TEM image of ZnO nanopencil recorded along the length is shown in Figure 2e, with the corresponding fast Fourier transformed electron diffraction (FFTED) pattern as an inset. The high resolution TEM image reveals distinct lattice fringe spacing, ~0.285 nm, which corresponds to the (002) plane of ZnO. From the HRTEM examination, highly structural perfection without any dislocations and planner defects is found. It suggests that growth of ZnO is taking place along the *c* axis corresponding to the [0001] direction (Figure 2e).

Figure 3 shows the morphologies of as-grown Sample III and Sample IV (hydrothermal treatment to the Sample III) investigated using FESEM. The well-aligned as-grown nanorods having orientation perpendicular to the Zn foil with relatively high cover density (Figure 3a). The as-grown ZnO nanorods are hexagonal in shape and have a diameter of ~80 nm. In the magnified view (Figure 3b), the faceted nanorods are clearly observed. After hydrothermal treatment to Sample III (Sample IV) at 120 °C for 12 h, we observed a highly covered dense surface with aligned nanorods perpendicular to the as-grown Sample III (Figure 3c). The magnified image shows the faceted nanorods with the prismatic tip at the one end which looks like nanopencil as shown in Figure 3d and an inset of Figure 3c. The diameter of these nanopencils is also observed to be ~80 nm. It is noteworthy that the diameter of rods in both samples is observed to be same, except sharp tapering at the end in Sample IV. Creation of such unique morphology using hydrothermal etching route is a single step process and much superior compared to the earlier reports.

Control experiments were performed using the same concentration of precursor (0.02 M) using the hydrothermal method at 85 °C for 12 h on bare Zn foil as well as sputter coated ZnO seed on Si and Au/Si-substrate. Figure 4a depicts the highly dense 1D ZnO nanorods of size 200–220 nm grown perpendicular to the Zn foil using a mixture of ethanol/H₂O (8:2). An inset of

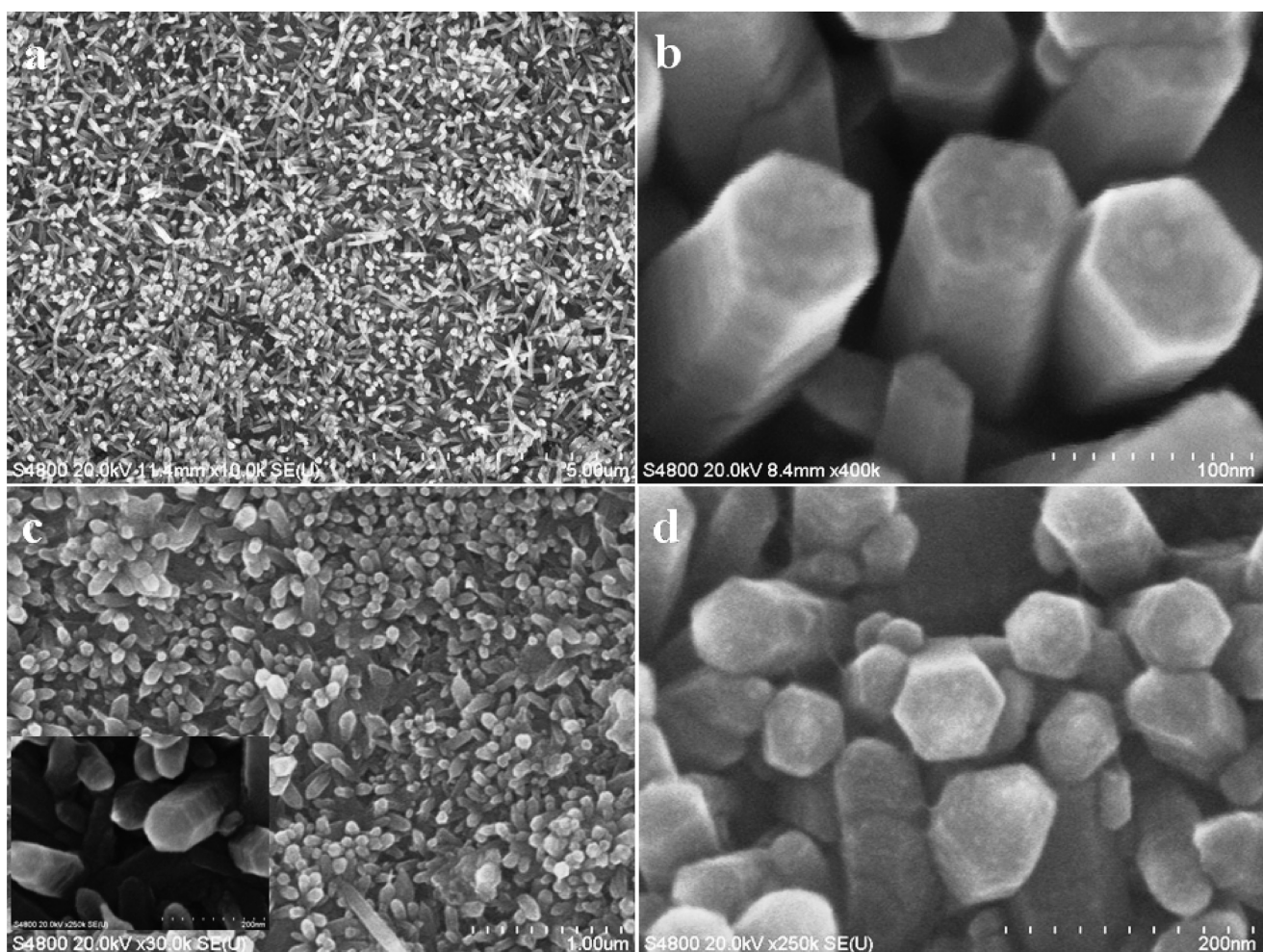


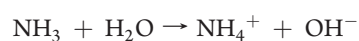
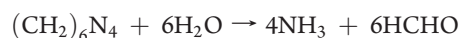
Figure 3. FESEM micrograph of Sample III (a,b) and (c,d) Sample IV (inset shows magnified view).

Figure 4a shows the magnified micrograph having symmetric tapering from base to top with blunt prismatic shape at the end of faceted rod. On the other hand, it shows only hexagonal ZnO nanorods of size 100 nm without prismatic shape (Figure 4b) when only an aqueous medium is used. Also, similar experiments were performed on as the deposited ZnO seed layer on Si and Au/Si-substrate using DC sputtering in order to reveal the role of ZnO seed layer (shown in Supporting Information S-IIb-c). Figure 4c depicts the SEM micrographs in which hexagonal 1D nanorods are grown perpendicular to the same Si-substrate. The diameter of these rods is in the range ~100–150 nm which show slight tapering at the end of the nanorods without faceted prismatic tips (inset of Figure 4c). Figure 4d depicts the SEM micrographs of hexagonal 1D nanorods grown perpendicular to the sputter coated ZnO on Au/Si-substrate of diameter ~100–150 nm. Surprisingly, at the top end of the faceted rod, pinholes of size 5 nm (see inset of Figure 4d) were obtained. Such unique nanostructures (faceted rods with pinhole) may be attributed to the presence of gold catalyst which is hitherto unattempted.

Hydrothermal synthesis is also performed using 0.01% cetyltrimethyl ammonium bromide (CTAB) as a capping agent under similar conditions as mentioned earlier. In this case, primarily, hexagonal ZnO nanodisc stacking was formed and further growth led into elongated bicones (Figure 5a). After a certain

reaction time, these bicones are broken into two parts due to excessive growth. (See Supporting Information S-IId.) On the surface of broken parts, spherical particles are seen in the range of 5–10 nm (inset of Figure 5a). Over a period of time, these broken parts join to form 2D nanostructures due to the secondary growth. Another controlled sonochemical reaction (instead of hydrothermal) for 90 min using 0.01 M precursor concentration (Figure 5b) demonstrated interesting 2-D hexagonal ZnO nanodiscs mostly perpendicular to the Zn substrate with thickness in the range of 5–7 nm.

Growth Mechanism. The formation of solid phase from a solution was proceeded through the nucleation and growth kinetics. When ultrasonication was provided to the reaction solution, the zinc hydroxide was formed which in turn converted into ZnO crystals. During nucleation, the clusters of nuclei were formed via rapid decomposition of precursors using ultrasonication and further the formation of particulate film of certain thickness by heterogeneous reactions at the substrate surface via crystal growth. The overall reaction mechanism can be represented by the following reactions:



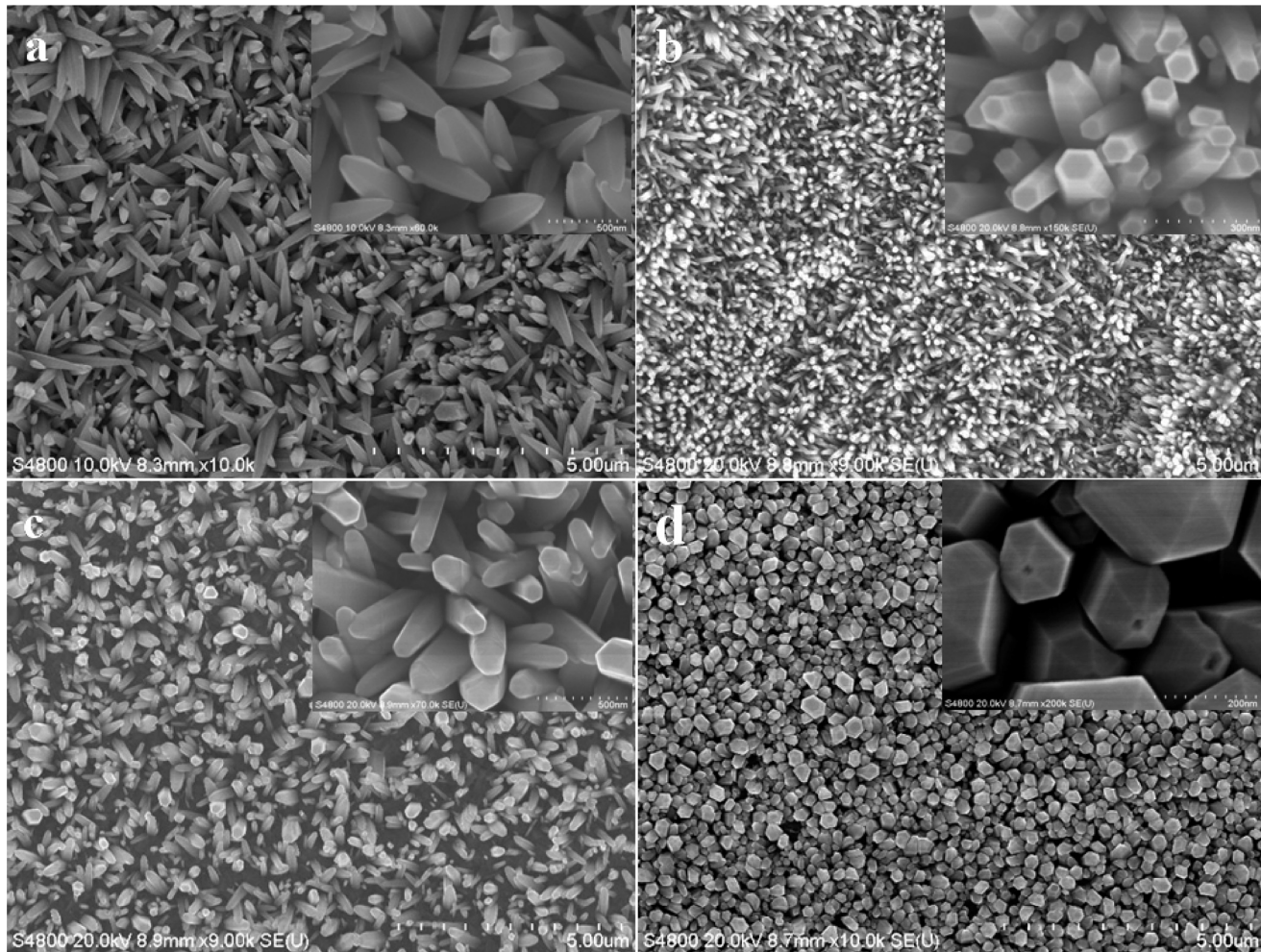
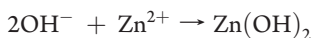


Figure 4. FESEM micrograph of ZnO nanorods (a) on Zn foil in a mixture of ethanol/H₂O = 8:2, (b) on Zn foil in H₂O (100 mL), (c) on sputter coated ZnO seed on Si-substrate in H₂O, and (d) on sputter coated ZnO seed on Au/Si-substrate in H₂O. (Insets show magnified view.)



The surface morphologies may greatly depend on the property of substrate surface, which is the key factor for chemical adsorption, if the surface of substrate is modified using seed layer which can serve as nucleation sites for the desired growth nanostructures. The important role of seed nuclei has been justified in the earlier reports.^{21,24} Induction of the seed layer effectively lowers the interfacial energy between the crystal nuclei and the substrate, which ultimately decreases the nucleation barrier and facilitates the growth of the ZnO nanostructures. Moreover, the seed layer also increases the surface roughness, resulting in the formation of more vacancies which promote the growth of the ZnO nanostructures. Recently, it was reported that the nonuniform seed layer exhibits growth of nanowires (bundles) along with different shaped crystals.²⁵

On the basis of experimental data obtained, the growth mechanism of the individual nanopencil can be explained by different growth rates of various ZnO crystal facets. In general, crystal growth is determined by a combination of original crystal related factors (intermolecular bonding preferences or dislocations) and external factors (supersaturation, solvents, time,

and additives).²⁶ ZnO is a polar crystal, and O²⁻ ions are in a hexagonal closed-packed (HCP) arrangement where with each Zn²⁺ lies within a tetrahedral group of four oxygen ions. Zn and oxygen atoms are arranged alternatively along the *c* axis, exhibiting a positive polar plane which is rich in Zn²⁺ while at the same time having a negative polar plane rich in O²⁻. The inherent asymmetry along the *c* axis leads to the anisotropic growth of 1D ZnO crystallites. The growth habit or morphology of the crystals depends on the relative growth rate of the different faces of the crystal, which in turn, depends on their interface structure. The growth rate along the radial axis should be slightly higher or nearly equal to the *c* axis, i.e., V [01 $\bar{1}$ 0] \geq V [0001].²⁷ This compensates the termination of OH⁻ along the *c* axis and maintains the uniform growth of rod, well-faceted with flat terminations. Samples I and III (flat termination) had a higher concentration of ZnO(OH)⁻ than Samples II and IV (one side prismatic termination).

The solvent also plays a key role in determining the different growth behavior of ZnO nanostructures. The interface–solvent interactions depend on surface energies of different crystal faces and solvent properties such as polarity, viscosity, and saturated vapor pressure.^{28–30} ZnO obtained using a mixture of ethanol/H₂O (8:2) after ultrasonication demonstrates the unidirectional growth due to the desired polarity of the reaction medium. Here,

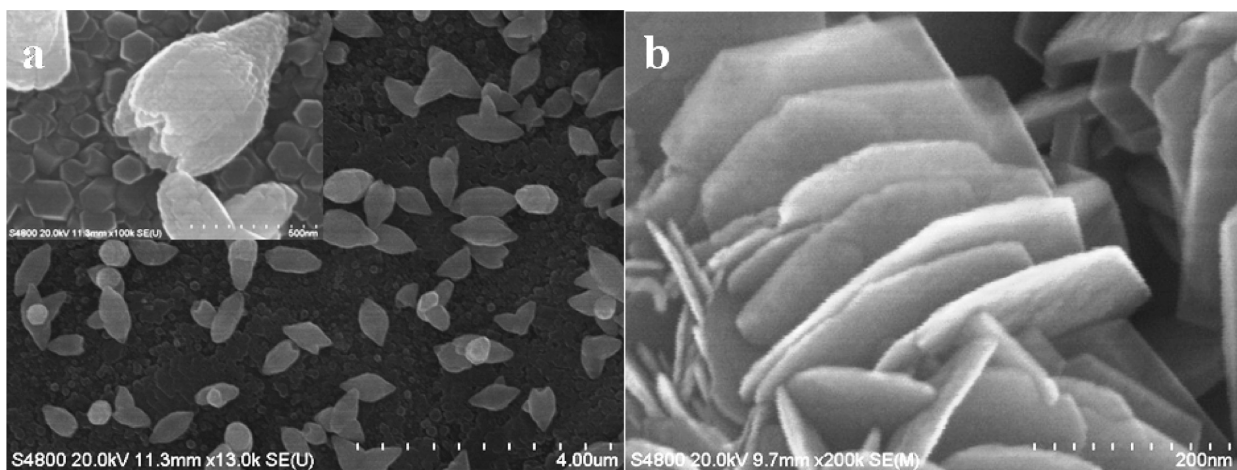
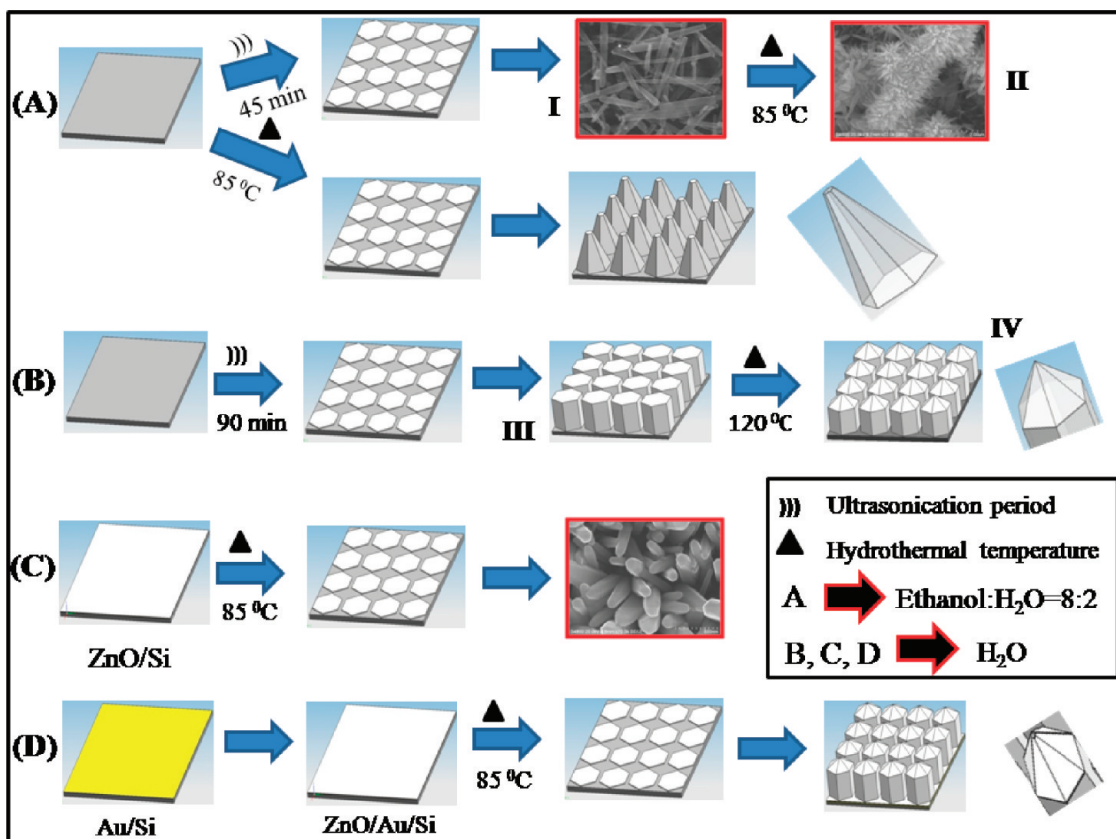


Figure 5. FESEM micrographs of ZnO nanostructures on Zn foil using (a) CTAB (0.01%) and (b) 90 min ultrasonication to the 0.01 M concentration.

Scheme 1. Schematic Illustration of ZnO Nanostructures



we observed that, when the polar solvent (H_2O) was added to ethanol, the dielectric constant of the reaction medium is increased which stabilizes the polar surface and impeded *c*-axis growth, which resulted in the formation of unidirectional ZnO nanorods which is mostly parallel to Zn substrate (Scheme 1A-I). After hydrothermal treatment, the evolution of ZnO nanorods into self-assembled ZnO nanopencils is accompanied by a dissolution–reprecipitation process, leading to the formation of urchin like nanostructures with a series of nanopencils around backbones (Scheme 1A-II). The formation of self-assembled

nanopencils is attributed to the high vapor pressure generated by 80% ethanol in reaction medium as well as growth of seed layer as mentioned earlier. However, without seed layer (without ultrasonication), hydrothermal treatment exhibits extremely different morphology, i.e., symmetric tapering of nanorods from base to top with blunt prismatic shape at the end of faceted rod (Scheme 1A).

When 0.02 M precursor solution was ultrasonicated for 90 min in the presence of clean Zn foil, the well faceted ZnO nanorods were grown on it. However, cavitations phenomenon due to

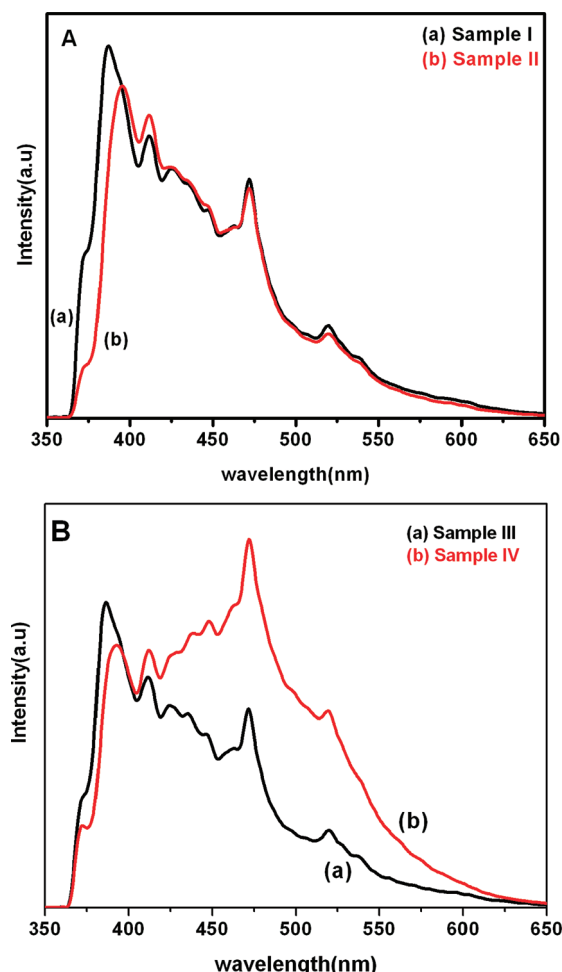


Figure 6. Room-temperature PL spectra of (A) Samples I and II and (B) Samples III and IV.

sonication compensates the termination of OH^- along the *c* axis and maintains highly uniform growth of rod, well-faceted with flat terminations (Scheme 1B-III). When these nanorods are used as a seed layer for further hydrothermal treatment at 120°C , well aligned 1D nanopencil are obtained (Scheme 1B-IV). Since the hydrothermal reaction is under constant vapor pressure of water for a period of 12 h, the growth rate along the radial axis should be slightly higher or nearly equal to the *c* axis, i.e., $V_{[01\bar{1}0]} \geq V_{[0001]}$. Hence, the one side prismatic termination obtained is quite understood due to higher concentration of $\text{ZnO}(\text{OH})^-$ than Sample II (Scheme 1A-II). When the ZnO seed layer is deposited on Si substrate using magnetron sputtering and treated for hydrothermal at 85°C , the 1D hexagonal nanorods perpendicular to the substrate are obtained. In this case, uniform faceted ZnO nanorods are obtained with blunt prismatic tip (Scheme 1C). As mentioned earlier, the seed layer contains a spherical particle. (See Supporting Information.) Initially, there is formation of hexagonal nanoplates via growth of ZnO seeds under hydrothermal conditions. The growth of uniform nanorods is due to the stacking of such hexagonal ZnO nanoplates obtained under hydrothermal conditions. After prolong reaction time, the concentration of Zn ions get reduced which ultimately suppress the growth of hexagonal plates. Hence, at the end of the rod, the obtained blunt prismatic shape is quite understood. The ZnO seed layer is obtained on Au coated Si

substrate using magnetron sputtering. The growth mechanism of ZnO nanorods is almost similar, as mentioned above except its different prismatic pinhole tip. The presence of gold acts as a catalyst, and it accelerates the growth of hexagonal ZnO nanorods. Hence, the diameter of the nanorods is slightly higher than the sputter coated Si-substrate. The cavity of ~ 5 nm obtained at the end of the prismatic rod may be due to gold catalyst. From the morphologies of the samples (Figure 4c,d), the effect of gold catalyst on the morphologies is clearly seen. Gold plays a vital role on the size of ZnO seed. The roughness of ZnO seed layer is observed more on Au/Si substrate compared with the Si substrate (which is shown in Supporting Information). The roughness of seed layer helps the fast growth of the ZnO nanorods. After complete growth, there may be dissolution of polar plane (002) at the tip to some extent to form a pinhole. However, further details of the mechanism of pinhole like ZnO nanopencils is under progress.

Photoluminescence (PL) spectroscopy is an effective technique for evaluating the optical properties of semiconductor materials. Figure 6 shows a typical room-temperature PL spectrum of all as-synthesized ZnO nanostructures. It consists of a near band edge peak at about 386 and 394 nm, etc., and a broad visible band with humps at about 411, 424, 435, 446, 470, 519, and 540 nm. On the other hand, the PL spectrum of the Samples I and III, prepared by ultrasonication, revealed a strong near band edge emission with remarkably low visible emissions. Such PL features indicate good crystallinity, lower lattice defects, and proper stoichiometry. In the case of Samples II and IV, there is a red shift in case of near band emission (NBE) by 8 nm. In addition, the relative intensity of the deep level emission (DE) peak has been increased for Sample IV. Relatively weak and broad UV emission along with blue-green emission observed in Sample IV (Figure 6B-b) implies that the optical properties of ZnO crystals are sensitive to the crystal morphology. Hence, we are reporting a larger shift in NBE of the ZnO due to a change in morphology. Normally, such shifts are observed due to doping.

The optical and field emission properties are enhanced with an increase in the aspect ratio. ZnO rods with flat ends were noticed in Samples I and III, and rods with sharp (prismatic or pyramidal) termination were noticed in Samples II and IV. The sharpness factor for the present case can be defined as the ratio of the height of pyramid to the size of the top flat surface ($S_f = h/b$). The sharpness factor for Sample II is better than Sample IV which suggests the sharp termination of the rods promoting the field emitter properties. In view of this, field emission study of ZnO with such unique morphology is performed.

The field emission current density versus applied field ($J-E$) curve of pin-cushion like ZnO cactus (Sample II) was shown in Figure 7. The specimen preconditioning, in terms of removal of any surface asperities and/or contaminants via ion bombardment by keeping the emitter at -2 kV with respect to the anode for 5 min duration, was carried out prior to $I-V$ measurement. The values of the turn-on field and threshold field, required to draw emission current density of 0.1 and $49 \mu\text{A}/\text{cm}^2$, are observed to be 1.38 and $2.84 \text{ V}/\mu\text{m}$, respectively. Since vertically aligned ZnO nanopencils have much smaller tips compared to the vertically aligned ZnO nanorods, it is reasonable that nanopencils show a smaller turn-on field than nanorods. These values of the turn-on and threshold field are found to be reproducible and are lower than that of reported ZnO nanostructures such as nanowires ($1.91 \text{ V}/\mu\text{m}$),³¹ nanoneedles ($2.4 \text{ V}/\mu\text{m}$),³² nanoppins ($1.92 \text{ V}/\mu\text{m}$),³³ and nanowalls ($3.6 \text{ V}/\mu\text{m}$).³⁴ The emission

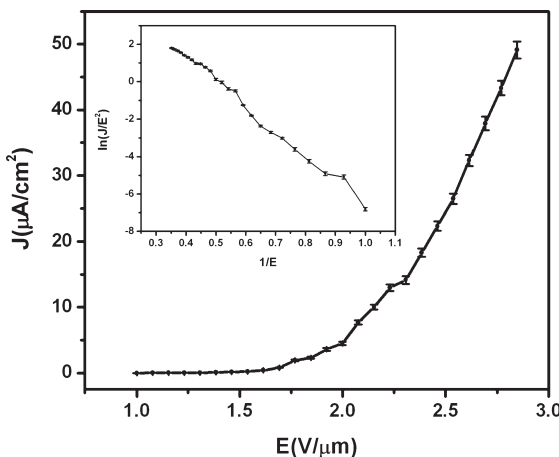


Figure 7. Field emission current density versus applied field ($J-E$) curve of the Sample II. The inset depicts the corresponding Fowler–Nordheim (F–N) plot.

current density versus applied field characteristic was analyzed by the Fowler–Nordheim (F–N) equation.³⁵ The inset of Figure 7 shows the corresponding $\ln(J/E^2)$ versus $(1/E)$ curve and the F–N plot derived from the observed $J-E$ characteristics. The F–N plot exhibits nonlinear behavior over the entire range of the applied field, indicating the semiconducting nature of the emitter. Similar nonlinear F–N plots have been reported for ZnO and other semiconductors.^{36,37} For semiconducting emitters, the observed nonlinearity can be understood on the basis of the band structure. It is believed that, initially, when the applied field is low, the emitted electrons originate mainly from the conduction band states, and as the applied field is increased, the valence band electrons also tunnel out and contribute to the emission current.³⁸

To understand our approach, it is necessary to have some idea of the theory behind it. Electrons in solid materials are confined by a potential-energy barrier. The potential energy of a planar cold cathode with microroughness can be written as

$$U(x) = -e^2/4x - \beta eEx + E_F + \Phi$$

where x is the distance away from the emitter surface, E_F is the energy of the Fermi level of the cathode materials, Φ is the potential barrier for the electron, e is the charge quantity of an electron, and E is the electric field strength directly on the emitter surface. The factor β is introduced to describe the geometric effect of the microroughness on the electric field. The tip emitter reduces the emission barrier width as compared to a planar surface. The relationship between FE current density and the applied electric field is described by the Fowler–Nordheim (F–N) equation:

$$J = A(\beta E)^2/\Phi \exp(-(\beta\Phi)^{3/2}/\beta E)^2$$

where A and B are constants. The field enhancement factor β in the F–N equation reflects the degree of FE enhancement of any tip over a flat surface: it represents the true value of the electric field at the tip compared to its average macroscopic value. For a nanostructural emitter, the β value is related to the geometry, crystal structure, conductivity, work function, and nanostructure density. According to the equations above, an effective approach to achieving strong electric fields is to employ sharp tips as

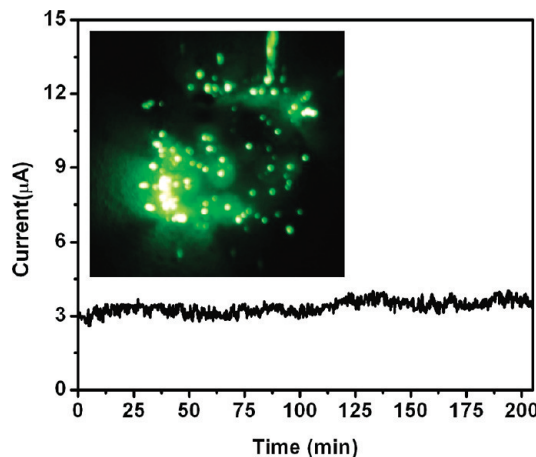


Figure 8. Field emission current stability ($I-t$) plot of the Sample II. The inset shows a typical field emission image.

electron emitters. In addition, lowering the electron barrier is beneficial to FE.

The field emission current stability of the ZnO nanopencils has been further investigated at a base pressure of $\sim 1 \times 10^{-8}$ mbar. The current versus time ($I-t$) plot for the same required duration of 3 h is shown in Figure 8. The emitter exhibits excellent emission current stability at $3 \mu\text{A}$, and the current fluctuations are observed to be within $\sim 5\%$ of the average value. The field emission image captured at the onset of the current stability measurement is shown as the inset of the Figure 8. The observed emission images exhibit a large number of “bright spots”, each corresponding to an emission site. This emission image is consistent with the emitter surface morphology. The post field emission surface morphology shows no deterioration of the emitter surface, indicating its mechanical robustness against ion bombardment and field-induced stress.

4. CONCLUSIONS

In a nutshell, single step and economical synthesis of hierarchical ZnO nanostructures with nanorods engendered into pin-cushion cactus along with nanopencils using a facile sonochemical assisted hydrothermal route at low temperature was demonstrated for the first time. Additionally, the unique morphologies like nanopencils with a pinhole, 2D hexagonal nanodiscs, bicones, and their different shapes have also been architected, successfully. We have studied field emission properties of pin-cushion cactus like ZnO nanopencil films which exhibits a low turn-on electric field of $\sim 1.38 \text{ V}/\mu\text{m}$. These results are better than the earlier reports of ZnO nanostructures. The field emitters prepared by the chemical route have been found to be quite stable with respect to the emission current and mechanical stability. All of these advantages may be useful in developing low cost field emission devices based on ZnO nanostructures in the future.

■ ASSOCIATED CONTENT

S Supporting Information. XRD spectra and FESEM micrographs of ZnO nanostructures. This material is available free of charge via the Internet at <http://pubs.acs.org>.

■ AUTHOR INFORMATION

Corresponding Author

*Tel.: +91 20 25692678 (M.A.M.); +91 20 25899273 (B.B.K.).
Fax: +91 20 25691684 (M.A.M.); +91 20 25898180 (B.B.K.).
E-mail: mam@physics.unipune.ac.in (M.A.M.); kbbb1@yahoo.com (B.B.K.).

■ ACKNOWLEDGMENT

The CMET authors gratefully thank the financial support from the Department of Information Technology (DIT), Delhi. We also thank Executive Director, C-MET, Pune.

■ REFERENCES

- (1) Rao, C. N.; Muller, A.; Cheetham, A. K. Recent development and new directions. In *Nanomaterials chemistry*; John Wiley: Hoboken, NJ, 2007.
- (2) (a) Edelstein, A. S.; Cammarata, R. C. *Nanomaterials: Synthesis, Properties and Applications*; Institute of Physical Publications: Bristol, UK, 1996. (b) Li, L.; Koshizaki, N.; Li, G. H. *J. Mater. Sci. Technol.* **2008**, *24*, 550.
- (3) Cui, Y.; Wei, Q. Q.; Park, H. K.; Lieber, C. M. *Science* **2001**, *293*, 1289.
- (4) Lee, C. Y.; Li, S. Y.; Lin, P.; Tseng, T. Y. *IEEE Trans. Nanotechnol.* **2006**, *5*, 216.
- (5) Jayadevan, K. P.; Tseng, T. Y. *J. Nanosci. Nanotechnol.* **2005**, *5*, 1768.
- (6) Law, M.; Greene, L. E.; Johnson, J. C.; Saykally, R.; Yang, P. *Nat. Mater.* **2005**, *4*, 455.
- (7) Li, S. Y.; Lee, C. Y.; Tseng, T. Y. *J. Cryst. Growth* **2003**, *247*, 357.
- (8) Lee, D. J.; Park, J. Y.; Yun, S. Y.; Hong, S. Y.; Moon, H. J.; Lee, T. B.; Kim, S. S. *J. Cryst. Growth* **2005**, *276*, 458.
- (9) Premkumar, T.; Zhou, Y. S.; Lu, Y. F.; Baskar, K. *J. Appl. Mater. Interfaces* **2010**, *2*, 2863.
- (10) Lee, C. Y.; Li, S. Y.; Lin, P.; Tseng, T. Y. *J. Nanosci. Nanotechnol.* **2005**, *5*, 1008.
- (11) Ahsanulhaq, Q.; Umar, A.; Hahn, Y. B. *Nanotechnology* **2007**, *18*, 115603.
- (12) Chang, Y. C.; Yang, W. C.; Chang, C. M.; Hsu, P. C.; Chen, L. J. *Cryst. Growth Des.* **2009**, *9*, 3161.
- (13) Wang, D.; Song, C. *J. Phys. Chem. B* **2005**, *109*, 12697.
- (14) Mo, M. S.; Wang, D.; Du, X.; Ma, J.; Qian, X.; Chen, D.; Qian, Y. *Cryst. Growth Des.* **2009**, *9*.
- (15) Li, B. Y.; Bando, Y.; Golberg, D. *Appl. Phys. Lett.* **2004**, *84*, 3603.
- (16) Dong, L. F.; Jiao, J.; Tuggle, D. W.; Petty, J. M.; Elliff, S. A.; Coulter, M. *Appl. Phys. Lett.* **2005**, *87*, 013110.
- (17) Wan, Q.; Yu, K.; Wang, T. H.; Lin, C. L. *J. Appl. Phys. Lett.* **2003**, *83*, 2253.
- (18) Banerjee, D.; Jo, S. H.; Ren, Z. *F. J. Adv. Mater.* **2004**, *16*, 2028.
- (19) Zhang, H.; Yang, D. R.; Ma, X. T.; Que, D. L. *J. Phys. Chem. B* **2005**, *109*, 1705.
- (20) Yao, I. C.; Lin, P.; Tseng, T. Y. *Nanotechnology* **2009**, *20*, 125202.
- (21) Warule, S. S.; Chaudhari, N. S.; Kale, B. B.; More, M. A. *CrystEngComm* **2009**, *11*, 2776.
- (22) Ramgir, N. S.; Late, D. J.; Bhise, A. B.; Mulla, I. S.; More, M. A.; Joag, D. S.; Pillai, V. K. *Nanotechnology* **2006**, *17*, 2730.
- (23) Cui, Q.; Huang, Y.; Zhu, Z. *Current Appl. Phys.* **2009**, *9*, 426.
- (24) Lui, Z.; Ya, J.; Lei, E. *J. Solid State Electrochem.* **2010**, *14*, 957.
- (25) Wen, B.; Huang, Y.; Boland, J. *J. J. Phys. Chem. C* **2008**, *112*.
- (26) Tong, Y.; Liu, Y.; Dong, L.; Zhao, D.; Zhang, J.; Lu, Y.; Shen, D.; Fan, X. *J. Phys. Chem. B* **2006**, *110*, 20263.
- (27) Li, W. J.; Shi, E. W.; Zhong, W. Z.; Yin, Z. W. *J. Cryst. Growth* **1999**, *203*, 186.
- (28) Li, F.; Ding, Y.; Gao, P.; Xin, X.; Wang, Z. L. *Angew. Chem.* **2004**, *116*, 5350.
- (29) Wang, C.; Shen, E.; Wang, E.; Gao, L.; Kang, Z.; Tian, C.; Lan, Y.; Zhang, C. *Mater. Lett.* **2005**, *59*, 2867.
- (30) Cheng, J. P.; Zhang, X. B.; Tao, X. Y.; Lu, H. M.; Luo, Z. Q.; Liu, F. *J. Phys. Chem. B* **2006**, *110*, 10348.
- (31) Jamali, S. F.; Joag, D. S.; More, M. A. *Ultramicroscopy* **2009**, *109*, 418.
- (32) Marathe, S. K.; Koinkar, P. M.; Ashtaputre, S. S.; More, M. A.; Gosavi, S. W.; Joag, D. S.; Kulkarni, S. K. *Nanotechnology* **2006**, *17*, 1932.
- (33) Xu, C. X.; Sun, X. W. *Appl. Phys. Lett.* **2003**, *83*, 3806.
- (34) Pradhan, D.; Kumar, M.; Ando, Y.; Leung, K. T. *Nanotechnology* **2008**, *19*, 35603.
- (35) Fowler, R. H.; Nordheim, L. W. *Proc. R. Soc. London, Ser. A* **1928**, *119*, 173.
- (36) Ramgir, N. S.; Mulla, I. S.; Pillai, V. K.; Late, D. J.; Bhise, A. B.; More, M. A.; Joag, D. S. *Appl. Phys. Lett.* **2006**, *88*, 42107.
- (37) Al-Tabbakh, A. A.; More, M. A.; Joag, D. S.; Ramgir, N. S.; Mulla, I. S.; Pillai, V. K. *Appl. Phys. Lett.* **2007**, *90*, 162102.
- (38) Al-Tabbakh, A. A.; More, M. A.; Joag, D. S.; Mulla, I. S.; Pillai, V. K. *ACS Nano* **2010**, *4*, 5585.